Bone Reports 12 (2020) 100246

Contents lists available at ScienceDirect

Bone Reports

journal homepage: www.elsevier.com/locate/bonr

6′-Methoxy Raloxifene-analog enhances mouse bone properties with reduced estrogen receptor binding

Katherine M. Powell[a], Alexa P. Brown[a], Cayla G. Skaggs[a], Alexis N. Pulliam[a], Alycia G. Berman[b], Padmini Deosthale[c], Lilian I. Plotkin[c], Matthew R. Allen[a,c], David R. Williams[d], Joseph M. Wallace[a,*]

[a] Department of Biomedical Engineering, Indiana University-Purdue University at Indianapolis, Indianapolis, IN, USA
[b] Weldon School of Biomedical Engineering, Purdue University, West Lafayette, IN, USA
[c] Department of Anatomy and Cell Biology, Indiana University School of Medicine, Indianapolis, IN, USA
[d] Department of Chemistry, Indiana University, Bloomington, IN, USA

ARTICLE INFO

Keywords:
Osteogenesis Imperfecta
SERM
Bone quality
Bone mechanics

ABSTRACT

Raloxifene (RAL) is an FDA-approved drug used to treat osteoporosis in postmenopausal women. RAL suppresses bone loss primarily through its role as a selective estrogen receptor modulator (SERM). This hormonal estrogen therapy promotes unintended side effects, such as hot flashes and increased thrombosis risk, and prevents the drug from being used in some patient populations at-risk for fracture, including children with bone disorders. It has recently been demonstrated that RAL can have significant positive effects on overall bone mechanical properties by binding to collagen and increasing bone tissue hydration in a cell-independent manner. A Raloxifene-Analog (RAL-A) was synthesized by replacing the 6-hydroxyl substituent with 6-methoxy in effort to reduce the compound's binding affinity for estrogen receptors (ER) while maintaining its collagen-binding ability. It was hypothesized that RAL-A would improve the mechanical integrity of bone in a manner similar to RAL, but with reduced estrogen receptor binding. Molecular assessment showed that while RAL-A did reduce ER binding, downstream ER signaling was not completely abolished. *In-vitro*, RAL-A performed similarly to RAL and had an identical concentration threshold on osteocyte cell proliferation, differentiation, and function. To assess treatment effect *in-vivo*, wildtype (WT) and heterozygous (OIM+/−) female mice from the Osteogenesis Imperfecta (OI) murine model were treated with either RAL or RAL-A from 8 weeks to 16 weeks of age. There was an untreated control group for each genotype as well. Bone microarchitecture was assessed using microCT, and mechanical behavior was assessed using 3-point bending. Results indicate that both compounds produced analogous gains in tibial trabecular and cortical microarchitecture. While WT mechanical properties were not drastically altered with either treatment, OIM+/− mechanical properties were significantly enhanced, most notably, in post-yield properties including bone toughness. This proof-of-concept study shows promising results and warrants the exploration of additional analog iterations to further reduce ER binding and improve fracture resistance.

1. Introduction

Current interventions used to reduce skeletal fragility focus on increasing bone mass rather than improving bone quality, intrinsic material properties of the tissue regardless of mass, size, or shape. Although increasing mass helps support bone's mechanical integrity, tissue quality is increasingly recognized as an important consideration. Bisphosphonates (BPs) have been the gold standard treatment for numerous bone disorders over the past 30 years (Russell, 2011; NIH, 2001; Glorieux et al., 1998). Although BPs improve bone mineral density, long-term use can have unintended consequences and can lead to negative quality-based changes such as microdamage accrual, increased non-enzymatic collagen cross-linking, and increased regions of non-viable osteocytes (Allen and Burr, 2008; Allen et al., 2008, 2006; Tang et al., 2009; Gourion-Arsiquaud et al., 2010). These negative quality-based changes have been correlated with reduced mechanical properties of bone tissue (Acevedo et al., 2015; Allen and Burr, 2011).

Bone quality can be quantified by measurements including, but not

* Corresponding author at: Indiana University-Purdue University at Indianapolis, Department of Biomedical Engineering, 723 W Michigan St. SL220D, Indianapolis, IN 46202, USA.
E-mail address: jmwalla@iupui.edu (J.M. Wallace).

https://doi.org/10.1016/j.bonr.2020.100246
Received 10 January 2020; Accepted 15 January 2020
Available online 17 January 2020

limited to, tissue mineral density, tissue hydration, chemical composition, enzymatic and non-enzymatic collagen cross-linking, collagen organization, or accumulation of microdamage. Changes to bone quality can have profound macroscopic mechanical effects (van der Meulen et al., 2001; Donnelly, 2011; Judex et al., 2003; Seeman and Delmas, 2006; Launey et al., 2010). It is well accepted that collagen quality in bone is directly related to bone ductility and toughness, properties that contribute to overall fracture resistance. Targeting collagen offers a unique therapeutic option when other treatments fall short.

Raloxifene (RAL) is in a class of drugs known as selective estrogen receptor modulators (SERM). In the past, RAL was used to treat osteoporosis in postmenopausal women and, clinically has been shown to reduce fractures by ~50% with only modest changes in bone mineral density (BMD) (Seeman et al., 2006; Recker et al., 2011; Ettinger et al., 1999). While RAL's primary mechanism relies on cell-dependent binding to osteoblasts through its high affinity for estrogen receptor alpha (ERα: one of the two main types of estrogen receptor) (Bryant, 2001), the compound has been shown to enhance bone material properties in a cell-independent manner by increasing tissue hydration at the collagen-mineral interface (Gallant et al., 2014; Bivi et al., 2016). These cell-independent, material-based changes induced by RAL are exciting from the perspective of presenting a unique way to improve fracture resistance in diseased bone, but RAL's estrogen-based effects pose challenges. As with estrogen treatment, RAL can lead to adverse reactions, such as hot flashes and increased thrombosis risk. There is also a risk of pulmonary embolism, cerebrovascular death, and RAL does not reduce the risk of non-vertebral fractures and hip fractures. The hormonal therapy also prevents its usage in some at-risk patient populations, including children with bone disorders such as Osteogenesis Imperfecta (Qaseem et al., 2017; Reid, 2015).

Osteogenesis Imperfecta (OI) is a genetic disease in bone with majority of the cases caused by a mutation in Type I collagen or related proteins involved in collagen synthesis and assembly. The mutated collagen leads to improper assembly of its triple helical structure, driving quality-based deficiencies in the collagen-mineral composite (Kuivaniemi et al., 1997; Pihlajaniemi et al., 1984; Rowe and Shapiro, 1998). These changes induce macroscopic effects and cause brittle bones and frequent fractures in patients suffering from the disease. BPs are currently used for treatment in children with OI. Although bone mass is increased in OI patients treated with BPs, tissue quality remains inferior, and it is unclear if BP treatment consistently improves long bone fracture resistance in this clinical population (Dwan et al., 2016).

The clinical use of a drug like RAL to combat fragility though changes in collagen quality holds much promise, but forward progress necessitates the development of novel analogs that produce the positive hydration effect in collagen without binding to estrogen receptors. These pursuits led to the synthesis of a first iteration Raloxifene Analog (RAL-A). The goal of creating this analog was to maintain the cell-independent effects of RAL, but abolish or reduce ER binding by altering key structural features of molecular recognition (Bivi et al., 2016). It was hypothesized that RAL-A would improve the mechanical integrity of bone in a manner similar to RAL, but with reduced estrogen receptor binding. In this study, the Osteogenesis Imperfecta murine (oim) model was used to investigate how treatment would impact the phenotype of a quality-based disease state (Carriero et al., 2014).

2. Materials and methods

2.1. Compound fabrication

The preparation of the 6-methoxyraloxifene derivative RAL-A (Fig. 1, structure **2**) utilized published procedures which have been devised for the synthesis of raloxifene itself (Ablenas et al., 2011; Grese et al., 1997). In this analog, the methoxy substituent has replaced the 6-hydroxy functionality of RAL (Fig. 1, structure **1**) which is thought to

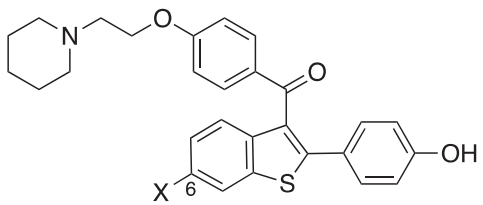

1 (X = OH)
2 (X = OCH_3) (RAL-A)

Fig. 1. Structures of RAL (**1**) and RAL-A (**2**). RAL possesses a 6-hydroxy substituent, while RAL-A possesses a 6-methoxy substituent.

mimic the A-ring hydroxylation present in estrogen and estradiol as a key feature for ER binding. The 6-methoxyraloxifene (RAL-A, **2**) was synthesized *via* the published procedures described for RAL (**1**) itself, starting with 4-methoxybenzaldehyde. Four steps were utilized to construct the RAL-A (**2**) beginning with the deprotonation of *N*,*N*-dimethylthioformamide for condensation with 4-methoxybenzaldehyde (Ablenas et al., 2011). Acid-catalyzed cyclization subsequently provided an intermediate benzothiophene for acylation and then conjugate addition of aryl Grignard reagent (Grese et al., 1997). In our case, the crude product was separated from other reaction byproducts using two successive flash column chromatographies [silica gel:ethyl acetate:hexanes (9:1 by volume) and then chloroform (100%)]. Clean fractions of the desired product were combined and solvent was removed *in vacuo* for subsequent recrystallization from ether:methanol to yield 4.0 g of yellow powder. Product RAL-A (**2**) was characterized by proton and carbon NMR spectroscopy and high-resolution mass spectrometry.[1] The RAL-A (**2**) was then converted into its hydrochloride (HCl) salt for increased water solubility in our biological studies. The HCl salt was obtained by passing anhydrous HCl gas through the diethyl ether solution of RAL-A (**2**), followed by evaporation of solvent under reduced pressure. The yellow HCl salt of RAL-A (**2**) (MW = 524.072) was a fine powder, characterized by proton NMR spectroscopy and stored at 22 °C under argon.[1]

2.2. Experiment #1: estrogen receptor binding assay

To assess the ability of RAL and RAL-A to bind to estrogen receptors (ER), a commercially available ERα-competitor assay was used (PolarScreen, Life Technologies). The ability of these compounds to bind to ERα and displace a fluorochrome tracer was measured using fluorescence polarization (EnVision 2102 Multilabel Plate Reader, Perkin Elmer) for compound concentrations ranging from 10^{-10} to 10^{-6} M. 17β-Estradiol was used as a positive control. Each concentration for each compound was measured in triplicate. The IC_{50}

[1] Characterization data for 6-methoxyraloxifene (RAL-A) and its corresponding HCl salt: **(2-(4-hydroxyphenyl)-6-methoxybenzo[b]thiophen-3-yl)(4-(2-(piperidin-1-yl)ethoxy)phenyl)methanone** ^{1}H NMR (600 MHz, Chloroform-d) δ 7.69 (d, J = 8.9 Hz, 2H), 7.62 (d, J = 8.9 Hz, 1H), 7.32 (d, J = 2.4 Hz, 1H), 7.21 (d, J = 8.6 Hz, 2H), 6.97 (dd, J = 8.9, 2.4 Hz, 1H), 6.69 (d, J = 8.9 Hz, 2H), 6.61 (d, J = 8.6 Hz, 2H), 4.08 (t, J = 6.0 Hz, 2H), 3.89 (s, 3H), 2.73 (t, J = 6.0 Hz, 2H), 2.51 (s, 4H), 1.61 (p, J = 5.6 Hz, 4H), 1.45 (p, J = 5.6 Hz, 2H); ^{13}C NMR (101 MHz, $CDCl_3$) δ 193.6, 162.8, 157.9, 157.2, 144.1, 140.2, 134.2, 132.6, 130.8, 130.3, 125.4, 124.3, 116.1, 115.0, 114.4, 104.7, 65.8, 57.7, 55.9, 55.1, 53.6, 25.5, 24.0. **(2-(4-Hydroxyphenyl)-6-methoxybenzo[b]thiophen-3-yl)(4-(2-(piperidin-1-yl)ethoxy)phenyl)methanone hydrochloride** ^{1}H NMR (400 MHz, Chloroform-d) δ 11.70 (s, 1H), 8.24 (s, 1H), 8.11 (d, J = 9.0 Hz, 1H), 7.49 (d, J = 8.2 Hz, 2H), 7.32 (d, J = 2.4 Hz, 1H), 7.08 (dd, J = 9.0, 2.4 Hz, 1H), 6.96 (d, J = 8.2 Hz, 2H), 6.67 (d, J = 8.1 Hz, 2H), 6.55 (d, J = 8.3 Hz, 2H), 4.51 (s, 2H), 3.91 (s, 3H), 3.58 (d, J = 11.0 Hz, 2H), 3.33 (s, 2H), 2.84 (s, 2H), 2.29 (d, J = 13.3 Hz, 2H), 1.93 (d, J = 12.9 Hz, 3H), 1.60 (s, 1H).

value, half of the maximal concentration the compound needs to fully displace the tracer, was obtained for each compound. A lower IC_{50} value indicates the compound is more potent and has a higher affinity for the receptor.

2.3. Experiment #2: in-vitro cellular function assessment

2.3.1. Cell culture

MC3T3-E1 Subclone 4 (ATCC® CRL-2593) murine pre-osteoblasts were obtained from the American Type Culture Collection (ATCC, Manassas, VA) and cultured in α minimal essential medium (α-MEM, Life Technologies, Carlsbad, CA) supplemented with 10% fetal bovine serum (FBS, GIBCO, Carlsbad, CA), 0.5% penicillin/streptomycin (GIBCO, Carlsbad, CA), 1% L-glutamine (Hyclone, Logan, UT), and 50 μg/ml ascorbic acid 2-phosphate (Sigma Aldrich, St. Louis, MO).

2.3.2. Cell proliferation assay

Cells were seeded into four 96-well plates (5,000 cells per well), corresponding to treatment periods of 1, 2, 3, or 7 days. Cells were allowed to adhere to the wells for 24 h prior to the start of treatment. Within each plate, cells were treated with one of six doses (0 nM, 1 nM, 10 nM, 100 nM, 1 μM, 10 μM) of RAL or RAL-A in 0.02% dimethylsulfoxide (DMSO; $n = 4$ per group). The CellTiter 96® AQueous One Solution Cell Proliferation Assay (Promega, Madison, WI) was used as a colorimetric method to determine the number of viable cells after the treatment period. At the end of each treatment period, 20 μL of CellTiter 96® One Solution Reagent was added to each well according to manufacturer instructions, and the plate was incubated for 2 h. The absorbance was then read at 490 nm using an ELx800 microplate reader (BioTek, Winooski, VT) to measure the soluble formazan produced from the cellular reduction of the reagent's tetrazolium compound, a measurement directly proportional to the number of living cells in culture.

2.3.3. Cell staining preparation

Cells were seeded into 24-well plates (60,000 cells per well). Cells were allowed to adhere to the wells for 24 h prior to the start of treatment. Starting with treatment, cells were cultured in mineralization media, which consisted of the media described above supplemented with 10 nM Dexamethasone and 10 mM β-glycerophosphate. Cells were cultured for 21 days with media changes every 2–3 days, during which time they were treated with one of six doses (0 nM, 1 nM, 10 nM, 100 nM, 1 μM, 10 μM) of RAL or RAL-A in 0.02% DMSO ($n = 3$ wells per group).

2.3.4. Alizarin red staining

The PromoCell protocol for Osteogenic Differentiation and Analysis of MSC was used for this assessment. To prepare the staining solution, 2 g of Alizarin Red was dissolved in 100 ml distilled water, mixed, adjusted to a pH between 4.1 and 4.3, and filtered. The medium was aspirated from the wells, and the cells were washed with Phosphate Buffered Saline (PBS; without Ca++/Mg++). The PBS was aspirated, then 10% neutral buffered formalin was added. After approximately 30 min, the formalin was removed and the cells were washed with distilled water. The Alizarin Red staining solution was added to the cells, and the plate incubated at room temperature in the dark for 45 min. The cells were washed 4 times with washing buffer, then imaged for qualitative analysis or staining.

2.3.5. Alkaline phosphatase staining

The PromoCell protocol for Osteogenic Differentiation and Analysis of MSC was used for this assessment. To prepare the staining substrate solution, one BCIP/NBT tablet (SigmaFastTM BCIP-NBT; Sigma Aldrich) was dissolved in 10 ml distilled water. Washing buffer was prepared by adding 0.05% Tween 20 to PBS. The medium was aspirated from the wells, and the cells were washed. 10% neutral buffered formalin was added for 60 s, at which time the cells were again washed with buffer. The cells were then covered with BCIP/NBT substrate solution and incubated at room temperature in the dark for 10 min. The cells were then washed with washing buffer and s imaged for qualitative analysis or staining.

2.4. Experiment #3: in-vitro C3 expression

2.4.1. Cell culture and treatment

MLO-Y4 osteocytic cells were cultured in phenol red-free α minimal essential medium supplemented with 2.5% fetal bovine serum/2.5% bovine calf serum and 1.0% penicillin/streptomycin. Cells were seeded into four collagen-coated 6-well plates (500,000 cells per well) in growing media and cultured overnight. After being given 24 h to adhere to the wells, media was removed and replaced with fresh media supplemented with 2% bovine serum albumin. The cells were cultured for an additional 25 min, then corresponding treatment was added to the wells in triplicate. Cells were treated with either RAL or RAL-A at concentrations of 10^{-7} M, 10^{-8} M, or 10^{-9} M. 17β-Estradiol (10^{-8} M) served as a positive control and DMSO served as the vehicle (final dilution of DMSO being 1:100 in each well). The cells were cultured for an additional 24 h, at which time mRNA was isolated as recommended (Kousteni et al., 2001).

2.4.2. RNA isolation and qPCR

Total RNA was isolated using TRIzol (Invitrogen, Grand Island, NY, USA), as previously published (Davis et al., 2017). Reverse transcription was performed using a high-capacity cDNA kit (Applied Biosystems, Foster City, CA, USA). qPCR was performed using the Gene Expression Assay Mix TaqMan Universal Master Mix and an ABI 7900HT real-time PCR system. The house-keeping gene glyceraldehyde 3-phosphate dehydrogenase (GAPDH, Applied Biosystems, Foster City, CA, USA ABI) was used. Primers and probes for C3 complement were designed using the Assay Design Center (Roche Applied Science, Indianapolis, IN, USA). Relative expression was calculated using the ΔCt method (Livak and Schmittgen, 2001).

2.5. Experiment #4: in-vivo animal study

2.5.1. Animals and treatment

All protocols and procedures were performed with prior approval from the Indiana University School of Medicine Institutional Animal Care and Use Committee. Female wild-type (WT) and heterozygous (OIM+/−) mice were bred from heterozygous parental strains on a C57BL/6 background (Carleton et al., 2008). Beginning at 8 weeks of age, mice ($n = 15$ per group) were subcutaneously injected with either RAL (0.5 mg/kg; 5×/week) or RAL-A (0.5 mg/kg; 5×/week). Solutions were prepared in 10% β-Cyclodextrin. Untreated controls were also included for each genotype. RAL dosage was chosen based on previous research showing efficacy *in-vivo*, and RAL-A dosage was chosen to match that of RAL (Allen et al., 2007, 2015; Berman et al., 2016). At 16 weeks of age, after 8 weeks of treatment, the mice were euthanized by CO_2 inhalation and right tibiae were harvested, stripped of soft tissue, and frozen in saline-soaked gauze at −20 °C.

2.5.2. Microcomputed tomography (μCT) and architectural analysis

To determine the effects of treatment on bone architecture, right tibiae were scanned using a nominal voxel size of 10 μm (Skyscan 1172, Bruker). Scans were performed using a 0.7-degree angle increment, two frames averaged, through a 0.5 mm Al filter ($V = 60$ kV, $I = 167$ μA). Images were reconstructed (nRecon) and calibrated to hydroxyapatite-mimicking phantoms (0.25 and 0.75 g/cm^3 Ca-HA). For each tibia, a cancellous region was selected at the proximal metaphysis and then quantified using CT Analyzer (CTAn). For consistency, the cancellous region started at the most distal portion of the proximal growth plate and extended distally 1 mm into the bone. To obtain cortical architectural properties, a 1 mm cortical region was selected at

approximately 50% length of the tibia, then analyzed with a custom MATLAB script (Berman et al., 2015).

2.5.3. Mechanical testing

Each tibia was tested to failure in four-point bending (upper loading span of 3 mm, lower support span of 9 mm) with the medial surface in tension. The bones were loaded at a displacement control rate of 0.025 mm/s while the sample remained hydrated with PBS. Cross-sectional cortical properties at the fracture location were obtained from μCT images as described above. These properties were used to map load-displacement data into stress-strain data using standard engineering equations derived from Euler-Bernoulli beam theory as previously reported to estimate tissue level properties (Wallace et al., 2009). Due to an error during the data acquisition process, some of the mechanical data were lost, resulting in n = 7–8 per group.

2.6. Statistical analysis

For the *in-vivo* study, all data were checked for assumptions of normality and homogeneity of variance, and violations were corrected using transformations. Within each genotype, a One-Way ANOVA with post-hoc Dunnett's test was used to statistically analyze the effect of each treatment *versus* control. Analysis was performed using GraphPad Prism (v.8) with a significance level at $\alpha = 0.05$. For the experiment using MLO-Y4 cells, a One-Way ANOVA followed by Tukey post-hoc test was performed.

3. Results

3.1. RAL and RAL-A similarly affected cellular behavior

RAL and RAL-A had no discernible impact on cell proliferation for any treatment period until the concentration of the compounds reached 10 μM (Fig. 2A and B). Qualitatively, cells were able to generate and mineralize a matrix, again until a concentration 10 μM, suggesting that neither compound impacted cell differentiation nor function (Fig. 2C).

3.2. RAL-A has reduced binding to ERα, but downstream ER pathway signaling is present

The results from the ERα binding assay (Fig. 3A) demonstrated an average IC_{50} value at 19.52 nM for the positive control, 17β estradiol. For RAL, the average IC_{50} value was 9.28 nM, while RAL-A produce an IC_{50} value nearly 20-fold of that at 183.2 nM. These results suggest that it took over an order of magnitude more of the raloxifene analog to displace the tracer and bind to ER. *In-vitro*, 17β estradiol binds to ER leading to downstream signaling as demonstrated by the increased expression of C3 (Fig. 3B). From 1 nM to 100 nM, there is C3 signaling present with RAL and RAL-A. For RAL-A, C3 expression trends upward with increasing concentration, reaching significance *versus* vehicle at 100 nM. These finding demonstrate that RAL-A is still able to signal through estrogen receptor in MLO-Y4 osteocytic cells.

3.3. RAL-A and RAL improve tibial trabecular microarchitecture

At the proximal metaphysis, bone volume fraction and bone mineral density were higher with RAL and RAL-A treatment in both OIM+/− and WT compared to their respective controls (Fig. 4A–F, Supplemental Table 1). Both treatments also generated higher trabecular thickness and trabecular number for each genotype. These changes led to a significantly lower trabecular separation in OIM+/− with RAL treatment (−10.7%) and a lower trend with RAL-A treatment (−8.4%, $p = 0.081$). Separation trended downward with RAL treatment in WT (−6.7%, $p = 0.12$) while RAL-A treatment led to a significant reduction (−9.5%). Tissue mineral density trended higher with treatment but failed to reach significance in either genotype (WT: $p = 0.063$; OIM+/−: $p = 0.106$).

At the mid-diaphysis, RAL and RAL-A had greater effects in OIM+/− than in WT (Fig. 4G–H, Table 1). Cortical thickness was significantly higher with RAL and RAL-A treatment in both genotypes. In WT, cortical area was significantly higher with RAL treatment (+15.5%) and trended upward with RAL-A treatment (+9.8%, $p = 0.083$). Cortical area was significantly higher in OIM+/− with both treatments. Total cross sectional area was also significantly higher with RAL-A treatment (+8.65%) but not changed with RAL (+7.22%, $p = 0.076$). Together, these changes led to significantly higher maximum moment of inertia in OIM+/− with both RAL and RAL-A

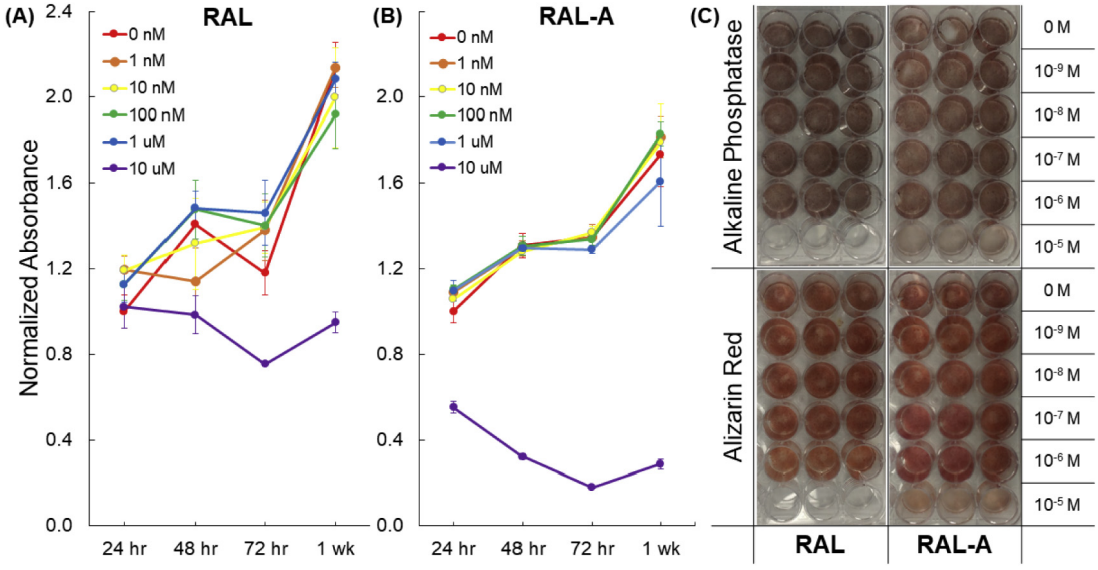

Fig. 2. Cells were treated with RAL (A) or RAL-A (B) at concentrations of 0 nM, 1 nM, 10 nM, 100 nM, 1 μM, and 10 μM. Absorbance was normalized to the 24 h 0 nM value for each compound. Cell proliferation had no qualitative impact until treatment reached 10 μM. (C) Alkaline Phosphatase and Alizarin Red staining for cells treated with RAL or RAL-A for concentrations at 0 nM, 1 nM, 10 nM, 100 nM, 1 μM, 10 μM. Qualitatively, cells were able to mineralize a matrix until treatment reached 10 μM.

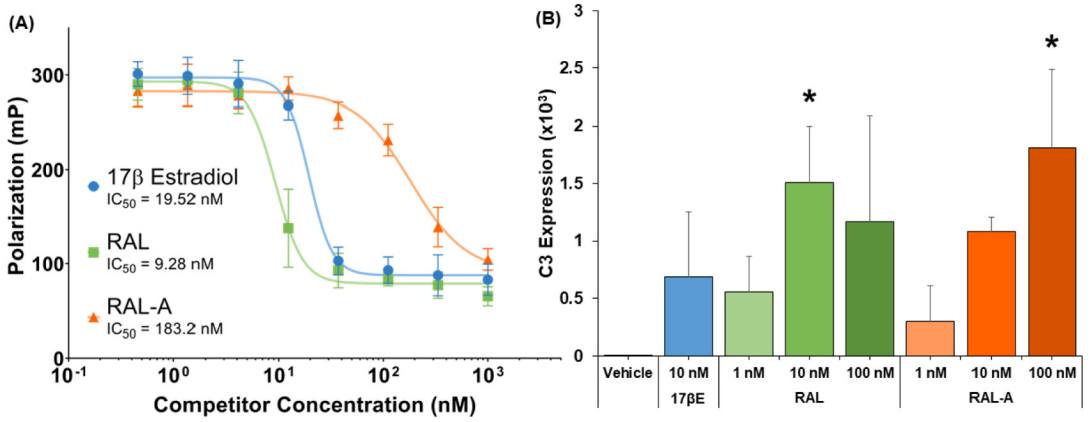

Fig. 3. (A) The ERα binding assay indicates the compounds ability to bind to ERα and displace a fluorochrome tracer, measured by fluorescence polarization. Polarization was measured for 17β estradiol, RAL, and RAL-A for concentrations ranging from 10^{-10} to 10^{-6} M. The IC_{50} value (50% tracer displaced) for 17β estradiol was 19.52 nM, RAL was 9.28 nM, and RAL-A was 183.2 nM. (B) Expression of C3 (multiplied $\times 1000$) in MLO-Y4 osteocytic cells after being treated with vehicle (DMSO), 17β estradiol (10^{-8} M), RAL (10^{-7}, 10^{-8}, and 10^{-9} M), or RAL-A (10^{-7}, 10^{-8}, and 10^{-9} M). A significant change from vehicle is indicated by '*' at $p < 0.05$. There was a significant increase noted for RAL at 10 nM and RAL-A at 100 nM compared to vehicle.

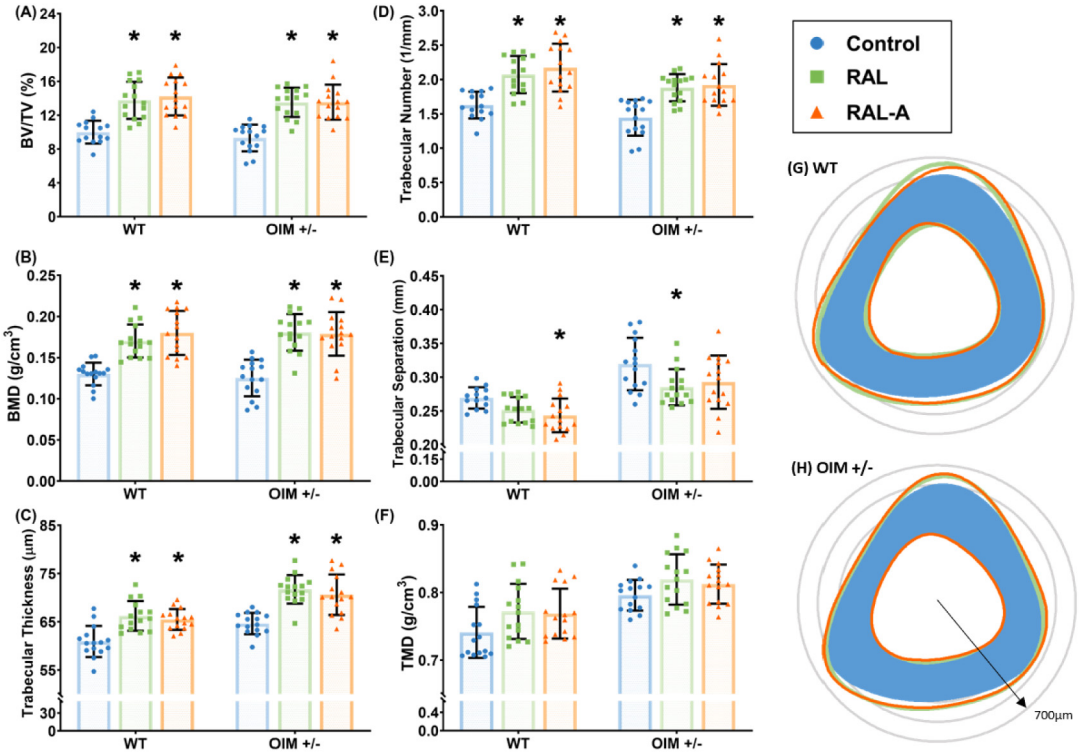

Fig. 4. Treatment effects on trabecular microarchitecture for (A) bone volume fraction (BV/TV), (B) bone mineral density (BMD), (C) trabecular thickness, (D) trabecular number, (E) trabecular separation, and (F) tissue mineral density (TMD). Significant change from control at $p < 0.05$ is indicated by '*' within each genotype. Schematic representation of the average cortical profile for each treatment group compared to respective control for (G) Wildtype and (H) Heterozygous OIM+/− samples.

treatments.

3.4. RAL-A and RAL enhanced post yield mechanical behavior in OIM +/−

As with the cortical properties noted above, mechanical effects were more apparent in OIM+/− (Tables 2 and 3, Fig. 5). Although some properties trended upward, treatment did not lead to any significant structural or tissue-level mechanical effects in WT compared to the control. For OIM+/− structural properties, RAL and RAL-A both led to similar changes. Both treatments produced significantly higher post-yield displacement and post-yield work. With RAL-A, this led to a non-significant but increasing trend in total displacement ($p = 0.07$) and total work ($p = 0.12$), while RAL produced a significant increase in these properties compared to control. At the tissue-level, RAL and RAL-A treatment increased total strain in OIM+/−. This contributed to increased toughness with both treatments compared to control in OIM +/− mice.

4. Discussion

Harnessing the cell-independent effects of Raloxifene in bone is a potential therapeutic option to target bone quality at the microscopic tissue level and improve mechanical integrity. However, RAL's cell-

Table 1
Cortical geometry at the tibial mid-diaphysis.

	WT									p-Value	OIM+/−									p-Value
	Control			RAL			RAL-A				Control			RAL			RAL-A			
	(n = 15)			(n = 15)			(n = 15)				(n = 15)			(n = 15)			(n = 15)			
Total CSA (mm^2)	0.95	±	0.07	1.03	±	0.12	0.99	±	0.09	0.223	0.852	±	0.036	0.914	±	0.063	0.926	±	0.05*	**0.038**
Marrow area (mm^2)	0.35	±	0.04	0.35	±	0.06	0.34	±	0.04	0.778	0.30	±	0.03	0.30	±	0.03	0.31	±	0.03	0.815
Cortical area (mm^2)	0.59	±	0.04	0.69	±	0.07*	0.65	±	0.05	**0.013**	0.55	±	0.01	0.62	±	0.05*	0.62	±	0.05*	**0.012**
Cortical thickness (mm)	0.213	±	0.008	0.240	±	0.01*	0.232	±	0.01*	**< 0.001**	0.211	±	0.006	0.232	±	0.01*	0.230	±	0.02*	**0.025**
Periosteal perimeter (mm)	4.20	±	0.20	4.37	±	0.31	4.28	±	0.23	0.439	3.98	±	0.08	4.10	±	0.14	4.14	±	0.11*	**0.045**
Endocortical perimeter (mm)	2.65	±	0.17	2.63	±	0.26	2.59	±	0.17	0.773	2.46	±	0.10	2.44	±	0.12	2.46	±	0.12	0.907
I_{max} (mm^4)	0.074	±	0.02	0.096	±	0.03	0.087	±	0.02	0.097	0.059	±	0.00	0.072	±	0.01*	0.074	±	0.01*	**0.009**
I_{min} (mm^4)	0.055	±	0.01	0.064	±	0.01	0.059	±	0.01	0.238	0.046	±	0.01	0.052	±	0.01	0.053	±	0.01	0.140
TMD (g/cm^3)	1.30	±	0.04	1.34	±	0.05	1.33	±	0.04	0.232	1.38	±	0.03	1.38	±	0.04	1.37	±	0.03	0.799

Values are presented as mean ± standard deviation. CSA - cross sectional area; I_{max} - maximum moment of inertia; I_{min} - minimum moment of inertia; TMD - tissue mineral density. A significant main effect of treatment within genotype is indicated by p-value at < 0.05. A significant difference compared to control indicated by '*' in the result columns.
P-values at < 0.05 are bolded as significant.

dependent effects as a SERM cause unintended side effects and make the drug unfit for use in some populations, including children. In this study, the goal was to create an analog of RAL which maintained the positive cell-independent effects on bone quality, but lacked the ability to bind to estrogen receptors and drive estrogenic signaling. Our rationale was to prepare a raloxifene analog that maintained the chemical and electronic properties of the parent drug, but altered RAL's 6-hydroxy substituent, affecting its capability as a hydrogen bond donor, an important feature for ER binding. Replacement with the 6-methoxy ether in RAL-A offered a direct, first generation derivative that also minimized the steric effects for substrate recognition. Further studies are needed to evaluate the role of electronic effects and steric bulk for C-6 substitution of the raloxifene parent structure. Overall, results indicate that RAL and RAL-A behave similarly *in-vitro* and *in-vivo*, but with reduced estrogen receptor binding with RAL-A. Although the binding was not completely abolished, this proof-of-concept study shows promising results and warrants the exploration of additional analog iterations to further reduce ER binding while still having positive effects on fracture resistance.

In-vitro, when osteoblasts were exposed to RAL and RAL-A across a range of concentrations, there were no discernable impacts of either compound on cell proliferation or differentiation (as measured through mineralization potential) until the concentration rose to 10 μM. This concentration threshold was similar for both compounds, and higher than treatments that would be used *in-vitro* or *in-vivo*. Utilizing an estrogen receptor competitor binding assay, it was shown that the binding of RAL-A to ERα was decreased by over an order of magnitude compared to both the 17β estradiol positive control and RAL. While the synthetic ERα binding assay indicated reduced ER binding with RAL-A, it was not completely abolished and some downstream ER signaling was still detected through C3 expression from cells treated with the compound. As future analogs are fabricated and tested, a more comprehensive analysis of ER signaling will be undertaken to verify reduced signaling prior to moving into *in-vivo* treatment studies.

RAL and RAL-A produced similar changes to tibial microarchitecture at both trabecular and cortical regions of interest. In both genotypes, the compounds increased trabecular bone volume fracture, number, and thickness as well as bone mineral density. In OIM+/−, cortical area, thickness, and maximum moment of inertia were all increased with both compounds as well. Similar geometric changes have been noted in the past with RAL treatment in male mice (Berman et al., 2016; Powell et al., 2019). However, the changes were not as pronounced as seen in this study with female mice. This could indicate that RAL is primarily acting as a SERM drug through its cell-dependent mechanism and promoting growth seen with estrogen receptor stimulation. Considering RAL-A resulted in similar architectural changes as RAL, it is likely that ER signaling is still prevalent with the analog, again supporting that more research is warranted to develop additional RAL iterations to minimize ER binding.

Animals treated with RAL and RAL-A also exhibited analogous

Table 2
Structural mechanical properties from 4-point bending of the tibial mid-diaphysis.

	WT									p-Value	OIM+/−									p-Value
	Control			RAL			RAL-A				Control			RAL			RAL-A			
	(n = 8)			(n = 7)			(n = 7)				(n = 8)			(n = 9)			(n = 7)			
Yield force (N)	14.6	±	2.722	17.01	±	1.8493	16.01	±	1.78	0.134	12.35	±	3.027	13.05	±	2.171	11.31	±	2.107	0.582
Ultimate force (N)	18.0	±	1.921	19.3	±	1.512	19.04	±	1.521	0.287	14.27	±	2.438	15.69	±	1.801	14.59	±	0.731	0.277
Displacement to yield (μm)	199.0	±	26.03	231.4	±	39.057	227.5	±	36.34	0.152	228.6	±	71.73	204.9	±	33.61	200.6	±	37.31	0.507
Postyield displacement (μm)*	393.1	±	207.5	404.7	±	169.03	458.7	±	100.1	0.732	119.1	±	82.83	293.9	±	108.9*	257.7	±	71.7*	**0.002**
Total displacement (μm)*	592.1	±	186.3	636.1	±	178.96	686.2	±	119.8	0.557	347.7	±	98.67	498.8	±	108.3*	458.3	±	82.57	**0.005**
Stiffness (N/mm)	81.9	±	10.28	82.8	±	15.364	79.51	±	17.13	0.907	62.1	±	13.66	72.33	±	14.85	63.21	±	7.745	0.218
Work to yield (mJ)	1.6	±	0.445	2.096	±	0.3804	1.971	±	0.36	0.067	1.59	±	0.762	1.454	±	0.372	1.249	±	0.446	0.496
Postyield work (mJ)*	5.6	±	2.276	6.721	±	3.0204	7.478	±	1.876	0.336	1.539	±	1.069	3.918	±	1.39*	3.13	±	0.71*	**0.001**
Total work (mJ)*	7.2	±	2.017	8.817	±	3.1509	9.45	±	2.091	0.207	3.129	±	1.408	5.372	±	1.36*	4.379	±	0.84	**0.005**

Values are presented as mean ± standard deviation. A significant main effect of treatment within genotype indicated by '*' in the property column. A significant difference compared to control indicated by '*' in the result columns.
P-values at < 0.05 are bolded as significant.

Table 3
Estimated tissue-level mechanical properties from 4-point bending of the tibial mid-diaphysis.

	WT							p-Value	OIM+/−							p-Value
	Control			RAL			RAL-A			Control			RAL			RAL-A			
	(n = 8)			(n = 7)			(n = 7)			(n = 8)			(n = 9)			(n = 7)			
Yield stress (MPa)	268.4	±	50.89	296.8	±	43.6	299	±	59.68	0.452	267.9	±	45.88	265.9	±	36.6	240.7	±	49.14	0.670
Ultimate stress (MPa)	331.1	±	43.24	337.1	±	44.4	352.6	±	45.02	0.637	311.5	±	33.54	320.3	±	25.07	310.5	±	26.64	0.696
Strain to yield (mε)	19.52	±	2.406	22.74	±	2.9	22.4	±	3.173	0.073	22.46	±	6.215	19.76	±	3.551	20.01	±	3.719	0.448
Ultimate strain (mε)	31.46	±	3.946	30.62	±	3.1	33.12	±	7.126	0.639	29.48	±	4.663	29.53	±	2.979	33.18	±	3.293	0.111
Total strain (mε)*	58.32	±	19.18	62.93	±	18.2	67.5	±	10.63	0.574	34.11	±	8.681	47.81	±	10.0*	45.77	±	8.59*	**0.008**
Modulus (GPa)	15.43	±	2.764	14.62	±	3.0	14.95	±	3.532	0.878	13.79	±	3.439	15.18	±	1.451	13.45	±	1.627	0.305
Resilience (MPa)	2.864	±	0.744	3.583	±	0.6	3.635	±	0.941	0.118	3.352	±	1.338	2.889	±	0.846	2.662	±	1.019	0.458
Toughness (MPa)*	13.37	±	4.83	14.95	±	4.8	17.22	±	3.896	0.286	6.488	±	1.734	10.61	±	2.88*	9.253	±	1.68*	**0.004**

Values are presented as mean ± standard deviation. A significant main effect of treatment within genotype indicated by '*' in the property column. A significant difference compared to control indicated by '*' in the result columns.
P-values at < 0.05 are bolded as significant.

changes in mechanical behavior. For both compounds, the effects were most pronounced in the diseased OIM+/− groups, and minimal treatment effects were observed in WT groups. This observation is likely because it is difficult to improve bone that is already of good or sufficient quality, as is the case in wild-type animals. In OIM+/−, perhaps the most notable finding is the increased toughness with RAL and RAL-A. Decreased post-yield behavior is a critical feature of the brittle phenotype associated with this OI model. In this case, increased toughness resulted from an increase in post-yield behavior, performance that is typically less dependent on bone mass and more related to the properties of the material itself (Boskey et al., 1999; Burstein et al., 1975; Wang et al., 2002; Garnero et al., 2006; Viguet-Carrin et al., 2006). Toughness is an estimated material property that has been normalized for bone size and shape. The increase in toughness noted here suggests that bone from the animals treated with RAL and RAL-A were able to absorb more energy before failure. Improvement of these properties in diseased OI bone gives further support for the need to pursue additional analogs. Similar increased post-yield behavior has been noted with RAL in *ex-vivo* soaking studies as well as RAL-treated female animals (Gallant et al., 2014; Allen et al., 2007; Berman et al., 2016). Conversely, assessment of mechanical properties from RAL-treated male mice of a similar age showed less compelling post-yield benefits of treatment (Berman et al., 2016; Powell et al., 2019). This discrepancy could indicate that ER signaling has a more important role, and further investigation of RAL and its analogs are needed in both sexes.

There are some limitations to this study. Due to data acquisition errors during mechanical testing, the sample size for each group was essentially cut in half. In both WT and OIM+/−, trends were present, but the unintentional loss of data and statistical power limited some of these properties from reaching significance. Even so, significant changes were present and compelling with the reduced sample size. Given the scope and duration of this study, adding additional animals to compensate for the loss was not an option. Future studies with other analog iterations will be powered to be able to detect these differences if they exist. Additionally, homozygous (OIM−/−) mice were originally included in this study. However, the severity of the phenotype caused numerous spontaneous fractures and only 3 control samples were usable for analysis.

Regarding study design, female mice were used here to model the current human population that most often uses RAL to determine if the analog would produce any SERM-like effects. Previous literature has demonstrated differences in ER activity between male and female mouse bone, and some even suggest that female mouse bones are more susceptible to changes in ERα activity (Nakamura et al., 2007; Sims et al., 2002; Saxon et al., 2012). Future studies should investigate the analogs in both female and male sexes to optimally reduce ER binding potential and isolate the cell-independent effects of RAL and RAL-A. Investigating both sexes could help determine if RAL-A is capable of enhancing bone mechanical integrity *in-vivo* without (or with reduced) ER binding. In addition, ER signaling will be investigated *in vivo*. In regard to *in-vitro* work, the impact on cells and ER binding should be investigated in all bone-related cell types (*i.e.* osteocytes, osteoblasts, and osteoclasts). This proof-of-concept study was not designed to

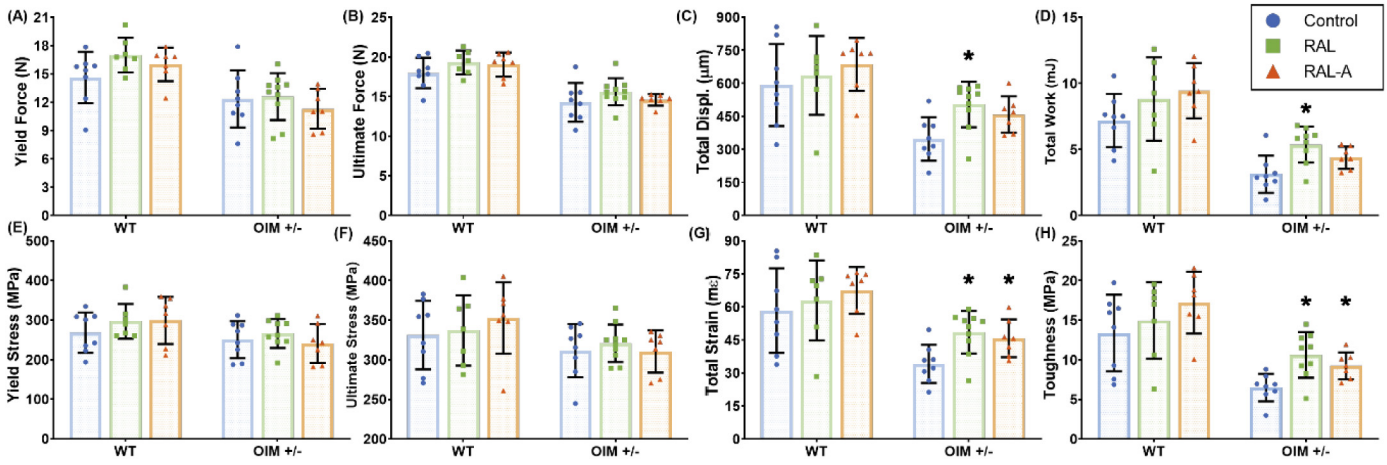

Fig. 5. Treatment effects on mechanical properties for (A) yield force, (B) ultimate force, (C) total displacement, (D) total work, (E) yield stress, (F) ultimate stress, (G) total strain, and (H) toughness. Significant change from control at $p < 0.05$ is indicated by '*' within each genotype.

directly compare the effects of *in-vivo* treatment on the quality of the bone extracellular matrix or levels of hydration. Future studies will incorporate additional techniques to assess quality changes at and below the microscopic level of bone, and bone matrix hydration. Measures of fracture toughness will also be evaluated.

In conclusion, this proof-of-concept study shows the potential benefit of using an analog of Raloxifene to enhance bone mechanical integrity while reducing the hormonal effects of estrogen therapy. By replacing an estrogen receptor binding motif on the compound, we were able to reduce, but not completely abolish, ER binding while still enhancing mechanical behavior in a manner similar to RAL. These results are exciting and demonstrate the need to investigate additional analog iterations of Raloxifene to minimize ER binding, enhance tissue quality, and improve bone health.

Declaration of competing interest

There are no known conflicts of interest associated with this publication, and there has been no financial support for this work that could have influenced its outcome.

Acknowledgements

We gratefully acknowledge Charlotte Phillips for the OI breeding colony. This work was supported, in part, by the NSF (AGB: DGE1333468), NIH (JMW: AR067221, AR072609), and IUPUI IPREP (ANP: GM109432).

Authors' roles

Study design: KMP, JMW, MRA, and AGB. Study Conduct: KMP, APB, CGS, PD, and DRW. Data Collection: KMP, APB, CGS, and PD. Data Analysis: KMP, PD, and JMW. Data Interpretation: KMP, JMW, AGB, MRA, and LIP. Drafting manuscript: KMP, JMW, DRW, and LIP. Revising manuscript content: KMP, JMW, DRW, MRA, ABG, and LIP. Approving final version of manuscript: KMP, APB, CGS, AGB, PD, LIP, MRA, DRW, and JMW.

Appendix A. Supplementary data

Supplementary data to this article can be found online at https://doi.org/10.1016/j.bonr.2020.100246.

References

Ablenas, F.J., George, B.E., Maleki, M., Jain, R., Hopkinson, A.C., Lee-Ruff, E., 2011. Destabilized carbocations. Nuclear magnetic resonance detection and reactivities of aryl α-thioformamidyl cations. Can. J. Chem. 65, 1800–1803.
Acevedo, C., et al., 2015. Alendronate treatment alters bone tissues at multiple structural levels in healthy canine cortical bone. Bone 81, 352–363 (Dec).
Allen, M.R., Burr, D.B., 2008. Mandible matrix necrosis in beagle dogs after 3 years of daily oral bisphosphonate treatment. J. Oral Maxillofac. Surg. 66 (5), 987–994 (May).
Allen, M.R., Burr, D.B., 2011. Bisphosphonate effects on bone turnover, microdamage, and mechanical properties: what we think we know and what we know that we don't know. Bone 49 (1), 56–65 (Jul).
Allen, M.R., Iwata, K., Phipps, R., Burr, D.B., 2006. Alterations in canine vertebral bone turnover, microdamage accumulation, and biomechanical properties following 1-year treatment with clinical treatment doses of risedronate or alendronate. Bone 39 (4), 872–879 (Oct).
Allen, M.R., Hogan, H.A., Hobbs, W.A., Koivuniemi, A.S., Koivuniemi, M.C., Burr, D.B., 2007. Raloxifene enhances material-level mechanical properties of femoral cortical and trabecular bone. Endocrinology 148 (8), 3908–3913 (Aug).
Allen, M.R., Gineyts, E., Leeming, D.J., Burr, D.B., Delmas, P.D., 2008. Bisphosphonates alter trabecular bone collagen cross-linking and isomerization in beagle dog vertebra. Osteoporos. Int. 19 (3), 329–337 (Mar).
Allen, M.R., et al., 2015. In vivo UTE-MRI reveals positive effects of raloxifene on skeletal-bound water in skeletally mature beagle dogs. J. Bone Miner. Res. 30 (8), 1441–1444 (Aug).
Berman, A.G., Clauser, C.A., Wunderlin, C., Hammond, M.A., Wallace, J.M., 2015. Structural and mechanical improvements to bone are strain dependent with axial compression of the tibia in female C57BL/6 mice. PLoS One 10 (6), e0130504.
Berman, A.G., Wallace, J.M., Bart, Z.R., Allen, M.R., 2016. Raloxifene reduces skeletal fractures in an animal model of osteogenesis imperfecta. Matrix Biol. 52–54, 19–28 (May-Jul).
Bivi, N., et al., 2016. Structural features underlying raloxifene's biophysical interaction with bone matrix. Bioorg. Med. Chem. 24 (4), 759–767 (Feb 15).
Boskey, A.L., Wright, T.M., Blank, R.D., 1999. Collagen and bone strength. J. Bone Miner. Res. 14 (3), 330–335 (1999/03/01).
Bryant, H.U., 2001. Mechanism of action and preclinical profile of raloxifene, a selective estrogen receptor modulation. Rev. Endocr. Metab. Disord. 2 (1), 129–138 (Jan).
Burstein, A.H., Zika, J.M., Heiple, K.G., Klein, L., 1975. Contribution of collagen and mineral to the elastic-plastic properties of bone. J. Bone Joint Surg. Am. 57 (7), 956–961 (in eng, Oct).
Carleton, S.M., et al., 2008. Role of genetic background in determining phenotypic severity throughout postnatal development and at peak bone mass in Col1a2 deficient mice (oim). Bone 42 (4), 681–694 (in eng).
Carriero, A., et al., 2014. How tough is brittle bone? Investigating osteogenesis imperfecta in mouse bone. J. Bone Miner. Res. 29 (6), 1392–1401 (Jun).
Davis, H.M., et al., 2017. Disruption of the Cx43/miR21 pathway leads to osteocyte apoptosis and increased osteoclastogenesis with aging. Aging Cell 16 (3), 551–563 (in eng, Jun).
Donnelly, E., 2011. Methods for assessing bone quality: a review. Clin. Orthop. Relat. Res. 469 (8), 2128–2138 (in eng, Aug).
Dwan, K., Phillipi, C.A., Steiner, R.D., Basel, D., 2016. Bisphosphonate therapy for osteogenesis imperfecta. Cochrane Database Syst. Rev.(10).
Ettinger, B., et al., 1999. Reduction of vertebral fracture risk in postmenopausal women with osteoporosis treated with raloxifene: results from a 3-year randomized clinical trial. Multiple Outcomes of Raloxifene Evaluation (MORE) Investigators. JAMA 282 (7), 637–645 (Aug 18).
Gallant, M.A., et al., 2014. Bone cell-independent benefits of raloxifene on the skeleton: a novel mechanism for improving bone material properties. Bone 61, 191–200 (Apr).
Garnero, P., et al., 2006. Extracellular post-translational modifications of collagen are major determinants of biomechanical properties of fetal bovine cortical bone. Bone 38 (3), 300–309 (in eng, Mar).
Glorieux, F.H., Bishop, N.J., Plotkin, H., Chabot, G., Lanoue, G., Travers, R., 1998. Cyclic administration of pamidronate in children with severe osteogenesis imperfecta. N. Engl. J. Med. 339 (14), 947–952 (Oct 1).
Gourion-Arsiquaud, S., Allen, M.R., Burr, D.B., Vashishth, D., Tang, S.Y., Boskey, A.L., 2010. Bisphosphonate treatment modifies canine bone mineral and matrix properties and their heterogeneity. Bone 46 (3), 666–672 (Mar).
Grese, T.A., et al., 1997. Structure-activity relationships of selective estrogen receptor modulators: modifications to the 2-arylbenzothiophene core of raloxifene. J. Med. Chem. 40 (2), 146–167 (in eng, Jan 17).
Judex, S., Boyd, S., Qin, Y.X., Miller, L., Muller, R., Rubin, C., 2003. Combining high-resolution micro-computed tomography with material composition to define the quality of bone tissue. Curr. Osteoporos. Rep. 1 (1), 11–19 (in eng, Jun).
Kousteni, S., et al., 2001. Nongenotropic, sex-nonspecific signaling through the estrogen or androgen receptors: dissociation from transcriptional activity. Cell 104 (5), 719–730 (in eng, Mar 9).
Kuivaniemi, H., Tromp, G., Prockop, D.J., 1997. Mutations in fibrillar collagens (types I, II, III, and XI), fibril-associated collagen (type IX), and network-forming collagen (type X) cause a spectrum of diseases of bone, cartilage, and blood vessels. Hum. Mutat. 9 (4), 300–315.
Launey, M.E., Buehler, M.J., Ritchie, R.O., 2010. On the Mechanistic Origins of Toughness in Bone. 40, no. 1. pp. 25–53.
Livak, K.J., Schmittgen, T.D., 2001. Analysis of relative gene expression data using real-time quantitative PCR and the 2-ddCT method. Methods 25 (4), 402–408 (in eng, Dec).
van der Meulen, M.C., Jepsen, K.J., Mikic, B., 2001. Understanding bone strength: size isn't everything. Bone 29 (2), 101–104 (in eng, Aug).
Nakamura, T., et al., 2007. Estrogen prevents bone loss via estrogen receptor α and induction of Fas ligand in osteoclasts. Cell 130 (5), 811–823 (2007/09/07).
NIH, 2001. Osteoporosis prevention, diagnosis, and therapy. JAMA 285 (6), 785–795 (Feb 14).
Pihlajaniemi, T., et al., 1984. Osteogenesis imperfecta: cloning of a pro-alpha 2(I) collagen gene with a frameshift mutation. J. Biol. Chem. 259 (21), 12941–12944 (Nov 10).
Powell, K.M., Skaggs, C., Pulliam, A., Berman, A., Allen, M.R., Wallace, J.M., 2019. Zoledronate and Raloxifene combination therapy enhances material and mechanical properties of diseased mouse bone. Bone 127, 199–206 (2019/10/01).
Qaseem, A., Forciea, M.A., McLean, R.M., Denberg, T.D., 2017. Treatment of low bone density or osteoporosis to prevent fractures in men and women: a clinical practice guideline update from the American College of Physicians. Ann. Intern. Med. 166 (11), 818–839 (in eng, Jun 6).
Recker, R.R., Mitlak, B.H., Ni, X., Krege, J.H., 2011. Long-term raloxifene for postmenopausal osteoporosis. Curr. Med. Res. Opin. 27 (9), 1755–1761 (Sep).
Reid, I.R., 2015. Efficacy, effectiveness and side effects of medications used to prevent fractures. J. Intern. Med. 277 (6), 690–706 (in eng, Jun).
Rowe, D.W., Shapiro, J.R., 1998. Osteogenesis Imperfecta. In: Metabolic Bone Disease and Clinically Related Disorders, 3 ed. Academic Press, pp. 651–683.
Russell, R.G., 2011. Bisphosphonates: the first 40 years. Bone 49 (1), 2–19 (Jul).
Saxon, L.K., Galea, G., Meakin, L., Price, J., Lanyon, L.E., 2012. Estrogen receptors alpha and beta have different gender-dependent effects on the adaptive responses to load bearing in cancellous and cortical bone. Endocrinology 153 (5), 2254–2266 (in eng, May).
Seeman, E., Delmas, P.D., 2006. Bone quality—the material and structural basis of bone strength and fragility. N. Engl. J. Med. 354 (21), 2250–2261 (in eng, May 25).
Seeman, E., Crans, G.G., Diez-Perez, A., Pinette, K.V., Delmas, P.D., 2006. Anti-vertebral

fracture efficacy of raloxifene: a meta-analysis. Osteoporos. Int. 17 (2), 313–316 (Feb).
Sims, N.A., et al., 2002. Deletion of estrogen receptors reveals a regulatory role for estrogen receptors-β in bone remodeling in females but not in males. Bone 30 (1), 18–25 (2002/01/01).
Tang, S.Y., Allen, M.R., Phipps, R., Burr, D.B., Vashishth, D., 2009. Changes in non-enzymatic glycation and its association with altered mechanical properties following 1-year treatment with risedronate or alendronate. Osteoporos. Int. 20 (6), 887–894 (Jun).
Viguet-Carrin, S., Garnero, P., Delmas, P.D., 2006. The role of collagen in bone strength. Osteoporos. Int. 17 (3), 319–336 (in eng).
Wallace, J.M., Golcuk, K., Morris, M.D., Kohn, D.H., 2009. Inbred strain-specific response to biglycan deficiency in the cortical bone of C57BL6/129 and C3H/He mice. J. Bone Miner. Res. 24 (6), 1002–1012 (Jun).
Wang, X., Shen, X., Li, X., Agrawal, C.M., 2002. Age-related changes in the collagen network and toughness of bone. Bone 31 (1), 1–7 (in eng, Jul).